Electronically preresonant stimulated Raman scattering microscopy in the visible

A. J. X. Choorakuttil ; A. Pruccoli ; M. J. Winterhalder ; P. Zirak ; D. Gudavičius ; G. Martynaitis ;
D. Petrulionis ; D. Samsonas ; L. Kontenis ; A. Zumbusch

Check for updates

CrossMark

View Online

Export Citation

Electronically preresonant stimulated Raman scattering microscopy in the visible

View Online   Export Citation   CrossMark

A. J. X. Choorakuttil,[1] (iD) A. Pruccoli,[1] (iD) M. J. Winterhalder,[1] (iD) P. Zirak,[1] (iD) D. Gudavičius,[2,3] (iD) G. Martynaitis,[2] (iD)
D. Petrulionis,[2] (iD) D. Samsonas,[2,4] (iD) L. Kontenis,[2] (iD) and A. Zumbusch[1,a)] (iD)

AFFILIATIONS

[1]Department Chemie, Universität Konstanz, 78457 Konstanz, Germany
[2]Light Conversion, 10233 Vilnius, Lithuania
[3]School of Physics and Astronomy, Cardiff University, Cardiff CF24 3AA, United Kingdom
[4]Laser Research Center, Physics Faculty, Vilnius University, 01513 Vilnius, Lithuania

[a)]Author to whom correspondence should be addressed: andreas.zumbusch@uni-konstanz.de

ABSTRACT

We report an experimental scheme for stimulated Raman scattering (SRS) microscopy with excitation in the visible spectral region. This allows electronically preresonant (epr) SRS microscopy of a broad range of chromophores with sensitivities as low as 1 μM. Our experiment is based on two synchronously near-infrared pumped optical parametric oscillators (OPO). One of the outputs is modulated at a fourth of the repetition rate with a novel broadband electro-optical modulator. Using a combination of spectral focusing and tuning of the OPO, we show the recording of epr-SRS spectra over the whole range of molecular vibrations at a speed up to 20 times faster than classical wavelength tuning. The imaging capabilities of this setup are demonstrated with material scientific and cellular samples.

Vibrational spectra of molecules are typically composed of many bands with widths of a few tens of cm^{-1} distributed over a range of 3000 cm^{-1}. This wealth of information allows the identification of molecules, which motivates the application of vibrational spectroscopy to the generation of molecule specific contrast in microscopy. Traditionally, this is done using infrared absorption in FT-IR microscopy[1] or spontaneous Raman scattering in confocal Raman microscopy.[2] Both methods, however, have drawbacks that are causes for their shadowy existence compared to fluorescence microscopy: Applications of FT-IR microscopy are hampered by low spatial resolution and the strong absorption of water, whereas spontaneous Raman microscopy suffers from sample autofluorescence and low sensitivity. During the last two decades, some of these limitations have been overcome by the development of non-linear Raman microscopy, i.e., coherent anti-Stokes Raman scattering (CARS) and stimulated Raman scattering (SRS) microscopy.[3,4] Sample autofluorescence is not a problem when using either of these methods, and image acquisition times are short since usually only one vibrational frequency is imaged at a time. Yet, the low sensitivity remains a problem also for these techniques.

An approach to achieve higher sensitivities is the recently demonstrated electronically preresonant (epr) SRS microscopy.[5,6] In SRS, a pump and a Stokes beam with frequencies ω_p and ω_S, respectively, are used to excite the sample [Fig. 1(a)]. A signal is observed when the frequency difference of both beams coincides with a vibrational transition of the sample molecules. When the excitation energies of pump and Stokes beams are chosen such that they additionally approach the energy of an electronic transition, the vibrational signal is electronically enhanced. This effect has been described theoretically by Albrecht and coworkers for electronically enhanced spontaneous Raman scattering.[7,8] The preresonance enhancement of the Raman scattering cross sections σ is usually dominated by the Albrecht A-term,[9]

$$\sigma = K\omega_p(\omega_S)^3 \left(\frac{\omega_p^2 + \omega_0^2}{(\omega_0^2 - \omega_p^2)^2} \right)^2, \qquad (1)$$

where K collects frequency-independent factors and ω_0 is the frequency of the electronic absorption.

With epr-SRS microscopy, detection sensitivities in the low μM range can be achieved, which corresponds roughly to one thousand molecules in the focal volume.[5,6,10,11] An important aspect of these experiments is that the excitation frequencies, ω_p and ω_S, have to be close to ω_0. A problem in this respect is that the laser systems used for
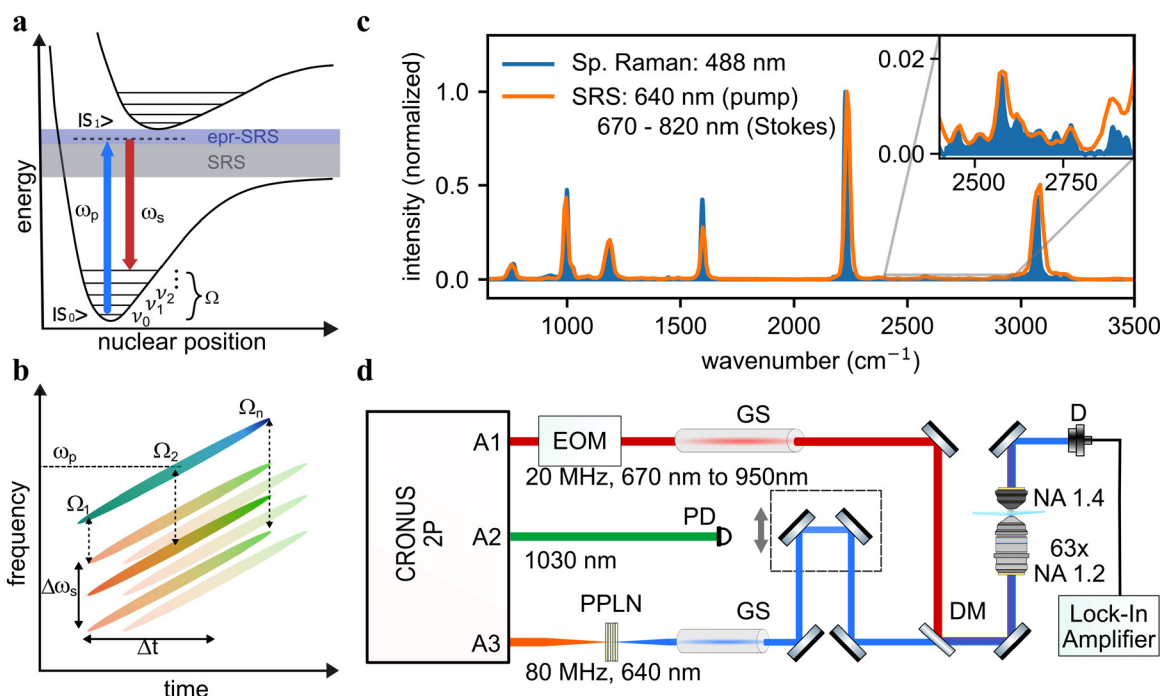
FIG. 1. (a) Energy diagram for SRS. (b) Time–frequency distribution of linearly chirped pulses with wavelength–time tunability. (c) Spontaneous Raman and SRS spectra of benzonitrile recorded by tuning the wavelength of the Stokes beam. (d) Scheme of SRS setup. A1: OPO tunable Stokes output, A2: fixed pump laser, A3: OPO output tunable from 960 to 1300 nm, EOM: electro optic modulator, PD: photodiode, PPLN: periodically poled lithium niobate crystal, GS: glass slab, DM: dichroic mirror, D: SRS detector.

SRS microscopy have to fulfill a number of other requirements: (i) high average power at high repetition rates; (ii) excitation pulse durations of approximately 1 ps; (iii) synchronization of pump and Stokes pulses; (iv) Stokes wavelength tunability independent from the fixed pump wavelength; and (v) low laser intensity noise. For standard SRS microscopy, most of these aims are met by using a ps near-IR pumped optical parametric oscillator (OPO). The fixed wavelength near-IR pump then serves as Stokes laser, and the signal output of the OPO is used as the tunable SRS pump laser.[12] For the detection of the SRS signal with a lock-in amplifier, one of the beams is preferentially modulated at half the repetition rate with an electro-optical modulator (EOM).[13] The disadvantage of using similar setups in epr-SRS microscopy is that only a very limited range of compounds with electronic resonances at the red edge of the visible spectrum can be investigated.[6] To date, two SRS experiments with excitation in the visible spectral range have been published.[11,14] In both cases, the spectra were only recorded over a range of approximately 200 cm^{-1}. A further complication arises from the fact that in these experiments, the pump beam wavelength was tuned to record SRS spectra. Since the pump beam provides the dominant contribution to the preresonant enhancement, changing its wavelength has a strong influence on the vibrational spectra.

Here, we report a method for broadband epr-SRS imaging with excitation in the visible region, using a combination of spectral focusing and wavelength tuning. Spectral focusing[15,16] allows us to record SRS spectra at high tuning speeds over short vibrational ranges [Fig. 1(b)], whereas the wavelength tuning of the central wavelength from the OPO extends the measurements over the whole vibrational

region with little influence on the preresonance enhancement. Since wavelength tuning of OPOs is slow, recording of an SRS spectrum in the finger print region ($\simeq 1000$ cm^{-1}) with acceptable spectral resolution (10 cm^{-1}) can take more than 30 min. In this work, we recorded SRS spectra up to 20 times faster by combining the wavelength tuning and the spectral focusing method. Figure 1(c) shows such an SRS spectrum of benzonitrile recorded by tuning the wavelength of the Stokes beam with step sizes of 100 cm^{-1}, from 600 to 3500 cm^{-1}.

The core of our setup [Fig. 1(d)] is a commercial laser system consisting of two synchronously pumped OPOs (CRONUS-2P, Light Conversion). The laser has three outputs: one at a fixed wavelength of 1030 nm, and two with wavelengths independently tunable between 670 and 960 and 960 and 1300 nm. The pulse durations are less than 160 fs for all outputs, and the repetition rate is 77.1 MHz. As is shown in Fig. 1(d), the SRS pump beam is obtained by frequency doubling of the longer wavelength tunable beam with a periodically poled lithium niobate crystal (PPLN, HC Photonics). The obtained pump beam was tunable between 625 and 650 nm. For epr-SRS experiments with molecules absorbing between 520 and 580 nm, we set the pump beam wavelength to 640 nm. The pump beam was sent over a delay stage before combination with the Stokes beam using a dichroic mirror. A water immersion objective (63×, NA 1.2, Leica Microsystems) served to focus the beams, and an oil immersion condenser (NA 1.4, Leica Microsystems) collected the light in the forward direction.

SRS signals were recorded from the in-phase component of the demodulated pump beam (Raman loss, SRL) using lock-in amplification (UHFLI, Zurich Instruments) with the 1030 nm output of the laser serving as a reference. The short wavelength laser output was

used as tunable Stokes beam modulated at 19.27 MHz with a broadband EOM. The broadband EOM is based upon two birefringent thermally compensated rubidium titanyl phosphate (RTP) crystals in a double pass configuration and a broadband Faraday isolator, which facilitates wavelength tuning. The isolator, in conjunction with significant and uneven acoustic heating of the RTP crystals at the 19.27 MHz pulse picking rate, limited the overall pulse-picker extinction ratio to less than 1:100. Broadband optical operation of the EOM over the whole laser output wavelength tuning range was achieved by adjusting the voltage applied to the crystals together with the changing wavelength. Unlike resonant EOMs, the EOM being used can pick single or multiple pulses from the 77.1 MHz pulse train at any rate below half the source rate.

The described laser system delivers nearly transform limited fs pulses. Due to the large spectral bandwidth of the pulses, their direct usage for SRS would result in a poor spectral resolution. An approach to circumvent this problem is spectral focusing, i.e., equal chirping of both excitation pulses.[15,16] The frequency difference between the chirped pump and Stokes beams can be tuned by changing the temporal delay between them. To match the typical width of vibrational lines in condensed phase, we aimed at a spectral resolution of less than 30 cm^{-1} for the SRS spectra. Pulses were chirped by using slabs of highly dispersive glass (H-ZF62, Gestione SILO).[16] SRS spectra of the sample molecules are then obtained in two different ways. To rapidly scan spectral regions of approximately 200 cm^{-1}, we simply changed the delay between pump and Stokes pulses. The spectral axis in this mode is also plotted as a temporal delay with the respective central frequency [Figs. 2(a) and 2(d) and Fig. 4(e)]. For scanning larger spectral ranges [Fig. 1(c)], we use a combination of spectral focusing and wavelength tuning, consisting in changes of the time delay (Δt) and the central wavelength of the Stokes (ω_S). To obtain regular Raman spectra from the spectral focusing data, the varying strength of the excitation field changes during the temporal scan has to be accounted for. For this purpose, we record the sum frequency (SF) between a pump and a
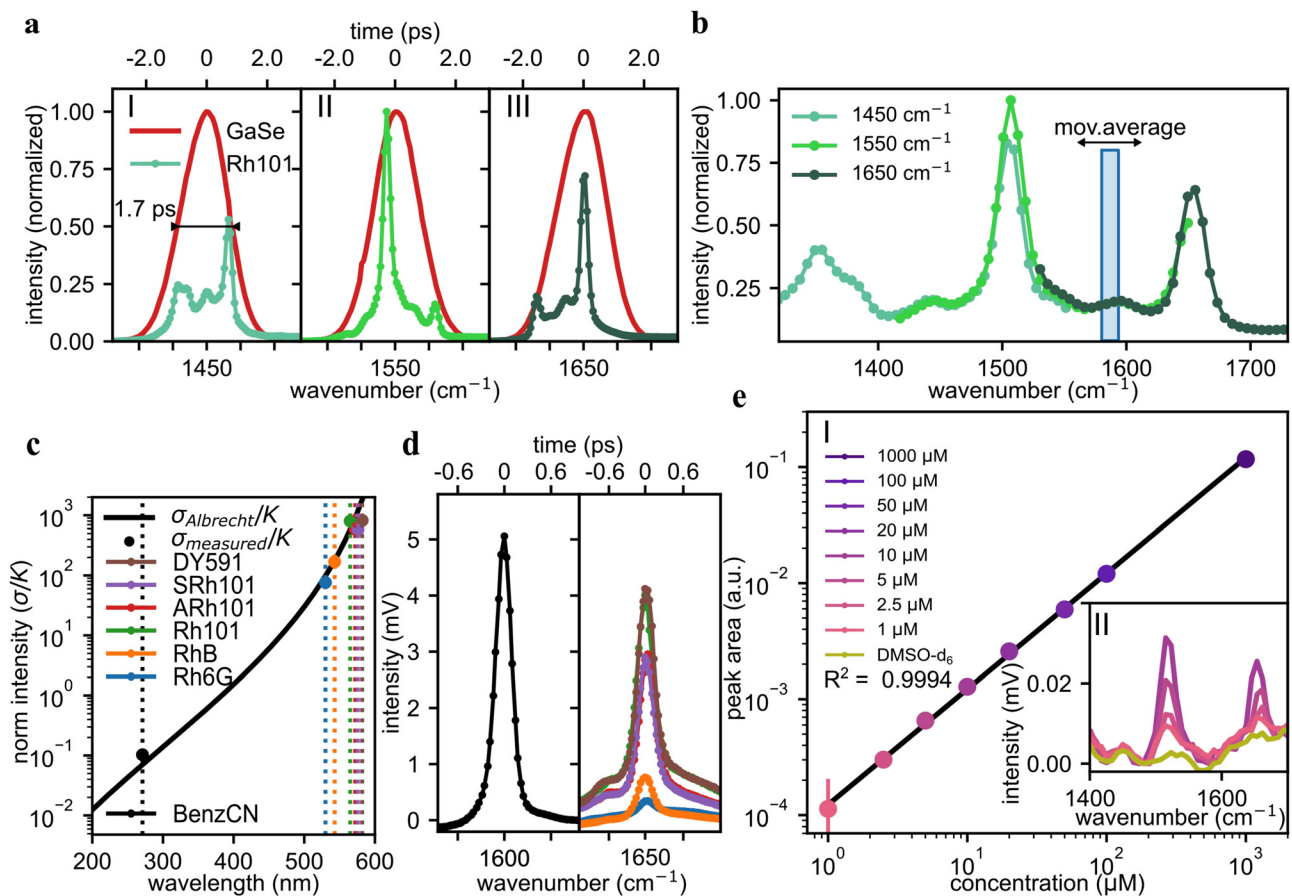
FIG. 2. (a) Spectral focusing spectra at different central wavelengths for 1 mM solution of Rh101 (green) compared with the pump loss signal from a crystal of GaSe (red), ticks every 100 cm^{-1}. (b) Reconstructed Raman spectrum from the traces presented in (a). (c) Calculated Albrecht A-term and measured intensity of the vibration at 1650 cm^{-1} for different absorbing dyes (listed in b) and benzonitrile at 1600 cm^{-1} excited with $\lambda_{pump} = 640$ nm. (d) Spectral focusing spectrum of 1 mM dyes solution centered at 1650 cm^{-1} and pure benzonitrile (BenzCN, $\lambda_{abs} = 271$ nm) centered at 1600 cm^{-1}: Rhodamine 6G (Rh6G, $\lambda_{abs} = 530$ nm), Rhodamine B (RhB, $\lambda_{abs} = 543$ nm), Rhodamine 101 (Rh101, $\lambda_{abs} = 565$ nm), AttoRhodamine 101 (ARh101, $\lambda_{abs} = 572$ nm), sulfoRhodamine 101 (SRh101, $\lambda_{abs} = 576$ nm), and DY-591 ($\lambda_{abs} = 582$ nm), ticks every 50 cm^{-1}. (e) SRh101 concentration dependence of the 1500 cm^{-1} peak area intensity after background correction. The spectra were recorded with a pump power of 13 mW, a Stokes power of 11 mW, and a lock-in time constant of 20 ms.

Stokes photon generated in a thin layer GaSe crystal as a pump loss in the SRL channel. The SF signal is used for both normalizing the intensity of SRS spectra and finding the time zero at every central wavelength point as shown in Fig. 2(a). Furthermore, a spontaneous Raman calibration sample is used to find the conversion factor between temporal and spectral resolution. The normalized spectra recorded at different central frequencies are merged together using a moving average with a step size of 8 cm^{-1}, Fig. 2(b). Combining this method with the fast tuning mode of the laser ($\simeq 15$ s per wavelength) allows us to record a spectrum over a range of 1000 cm^{-1} in 160 s.

Figure 2(c) shows a comparison between the experimental and theoretical results from Eq. (1) for the 1650 cm^{-1} band in the SRS spectra of six different rhodamine based dyes absorbing in the preresonant region and the 1600 cm^{-1} peak of benzonitrile, respectively. The two bands shown in Fig. 2(d) correspond to the totally symmetric stretching of the xanthene ring in the dyes and of the benzene ring in benzonitrile.[17,18] To give better insight into the enhancement factors, Fig. 2(d) depicts the SRS spectra for 1 mM solutions of the dyes compared to pure benzonitrile (this corresponds to 9.7 M). As expected, the dyes with electronic absorption closest to the pump wavelength exhibit the highest enhancement. Their SRS signal strength resembles that of the band of the 10^4 times higher concentrated benzonitrile. Figure 2(e) shows that the preresonance enhancement of the signals increases the SRS sensitivities to 1 μM. It is, however, important to note that these measurements are accompanied by mainly two types of background. The first is mixed two photon absorption (TPA) that occurs when one photon from the Stokes and one from the pump beam are absorbed simultaneously by the sample molecules. This results in a pump loss signal that is detected as vibrational frequency-independent background.[10] The second background source is due to cross phase modulation (XPM) caused by the optical Kerr effect and has previously been reported in other SRS experiments.[19,20] In this case, the pump loss signal arises due to transient scattering of the pump beam caused by a Stokes beam induced change in refractive index. Both of these backgrounds are much broader than the vibrational bands and can be removed by background subtraction with a Gaussian fit to the background to obtain the pure SRS signal that scales linearly with concentration [Fig. 2(e-I)].

We evaluated the imaging performance of our experimental setup by microscopy studies of polymer test samples and of fixed biological cells. First, a sample of three different types of 2 μm polystyrene (PS) beads was measured at different vibrational resonances with the aim of distinguishing them using epr-SRS. The beads were commercial PS beads labeled with an unknown dye with an electronic absorption at 580 nm (FluoroSpheres F-8801, ThermoFisher Scientific), commercial PS beads (Polysciences) dyed by encapsulating SolventRed197, a weakly fluorescing dye with an absorption maximum at 550 nm, following the procedure reported by Behnke et al.,[21] and undyed sulfate-modified polystyrene microspheres (Polysciences). SRS and spontaneous Raman spectra were recorded for each type of beads and are depicted in Fig. 3(a). The SRS images of the beads in water were recorded with excitation powers of 3.2 mW at the pump wavelength of 640 nm and of 12.8 mW at varying Stokes wavelengths, Fig. 3(b). The band at 1000 cm^{-1} originates from the PS matrix present in all beads. At 1500 cm^{-1}, only the FluoroSpheres are in resonance, whereas at 1580 cm^{-1}, SolventRed197 has the strongest resonance that, however, appears low in intensity due to the lower preresonance enhancement and possibly also a lower dye concentration than in the FluoroSpheres. Due to the onset of the strong resonance at 1600 cm^{-1}, the latter are still visible at 1580 cm^{-1} but with less intensity than when excited at 1500 cm^{-1}. The image taken off resonance at a Raman shift of 1760 cm^{-1} was used to subtract the SRS background from the other images. By comparison, the fluorescence signal recorded simultaneously with the SRS signal and allows the detection of the FluoroSpheres, but not of the undyed nor the weakly fluorescent SolventRed197 beads.
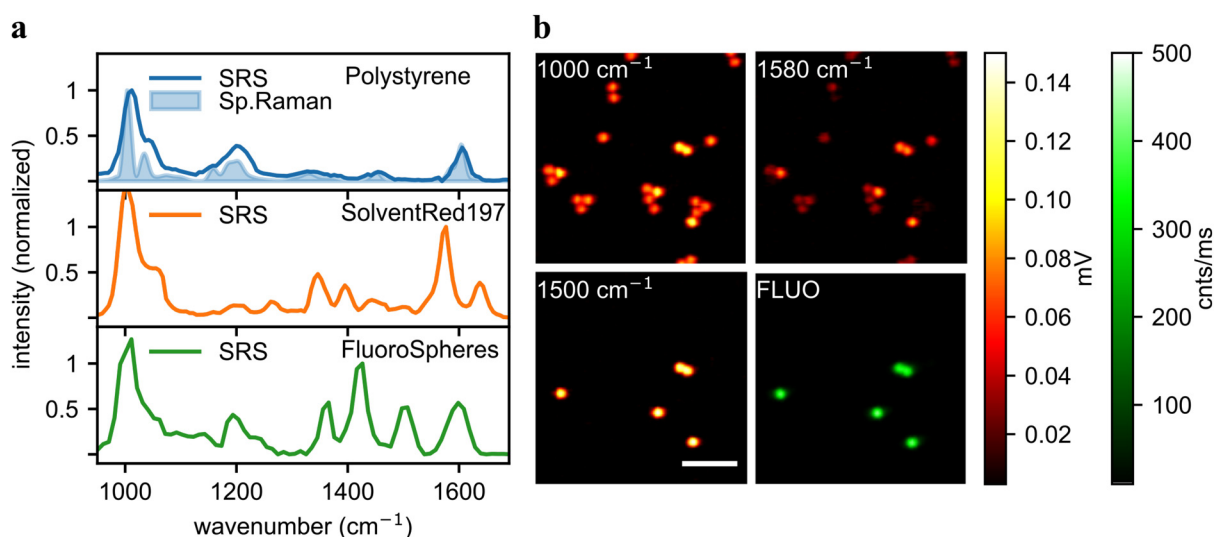
FIG. 3. (a) Spontaneous Raman and SRS spectra of polystyrene (PS) (blue). Epr-SRS spectra of SolventRed197 (orange) and FluoroSpheres in DMSO-d$_6$ (green), normalized with the molecule of interest maximum peak. (b) SRS images of dyed and un-dyed 2 μm PS beads (red): 1000 cm^{-1} (all beads in resonance), 1580 cm^{-1} (SolventRed197 and FluoroSpheres dyed beads in resonance), 1500 cm^{-1} (only FluoroSpheres dyed beads in resonance), and simultaneously recorded fluorescence image (green). Images were recorded with a pump power of 3.2 mW, a Stokes power of 12.8 mW, and a time constant of 1 ms for both the fluorescence and the SRS signal. Scale bar: 10 μm.
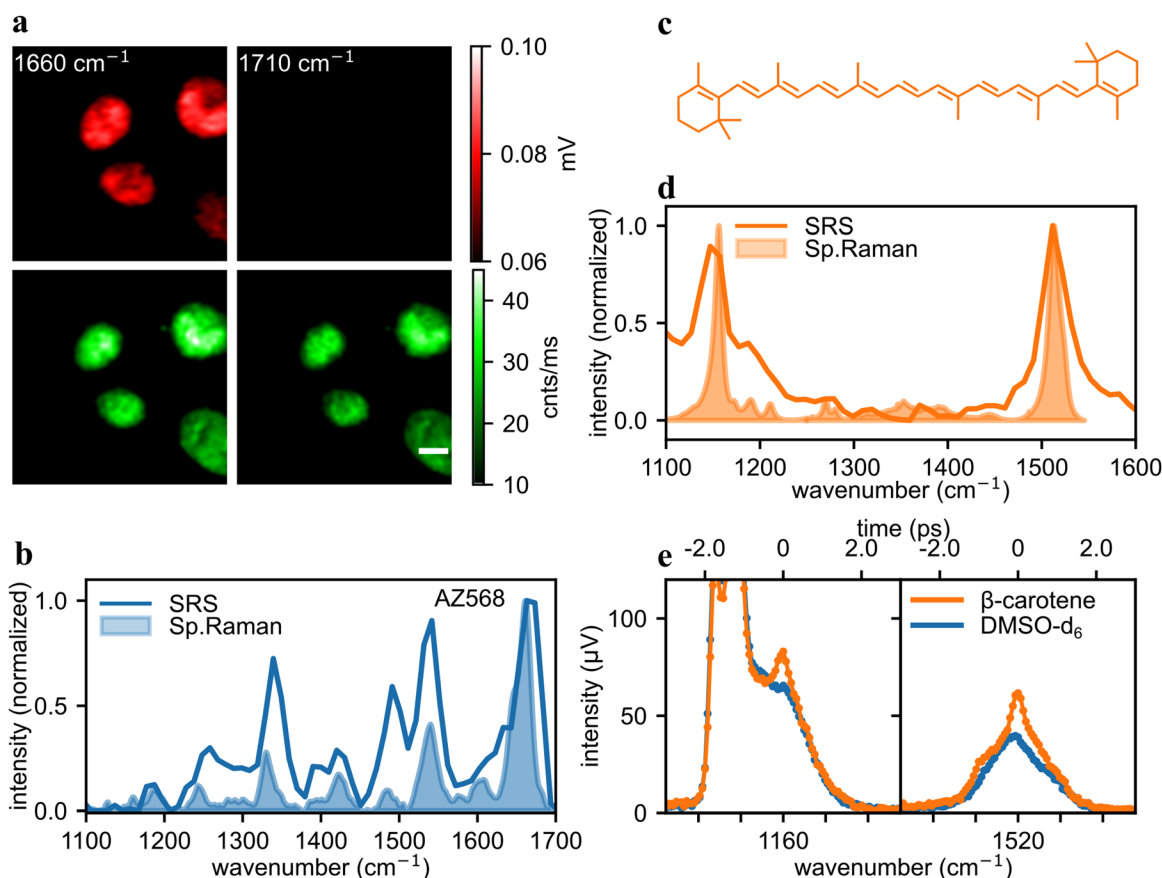
FIG. 4. (a) Imaging of nuclei of AZ568 stained, fixed HeLa cells with SRS (red) and fluorescence (green). Scale bar: 10 μm. (b) SRS and spontaneous Raman spectrum (at 488 nm) of 1 mM solution of AZ568 in DMSO-d_6. (c) Structure of β-carotene. (d) β-Carotene spectrum recorded with SRS (0.4 mM solution in DMSO-d_6) and spontaneous Raman (solid with 488 nm). (e) Spectral focusing spectrum centered at 1160 cm^{-1} of a 18 μM solution of β-carotene in DMSO-d_6 (orange) and pure DMSO-d_6 (blue), ticks every 100 cm^{-1}. The images were recorded with a pump power of 3 mW, a Stokes power of 17 mW, and a time constant of 1 ms for both the fluorescence and the SRS signal. The SRS spectra were recorded with a pump power of 8 mW, a Stokes power of 17 mW, and a time constant of 20 ms.

Finally, we used the epr-SRS setup to image labeled biological cells. To this end, we stained the nucleus of fixed HeLa cells with AZ568 functionalized with dibenzocyclooctyne (AZDye 568 DBCO, Fluoroprobes). The dye has an absorption maximum at 578 nm and is suited for bioorthogonal labeling through strain-promoted azide–alkyne cycloaddition [Fig. 4(a)].[22] The SRS and spontaneous Raman spectrum of the compound in Fig. 4(b) indicate a strong resonance at 1660 cm^{-1}. We recorded epr-SRS images at this resonance and off resonance at 1710 cm^{-1} simultaneously with the fluorescence images. While the fluorescence images remain unaffected by the wavelength shift, the vibrational resonance completely disappears. Since electronic preresonance enhancement does not require fluorescent sample molecules,[23] extending epr-SRS to visible excitation wavelengths is also interesting for the investigation of naturally occurring compounds in unlabeled biological samples. As an example, we recorded spontaneous Raman and epr-SRS spectra of (nonfluorescent) β-carotene [Figs. 4(c) and 4(d)]. Its main vibrational resonances are located at 1160 and 1520 cm^{-1}. While the absorption maximum of β-carotene is more than 5000 cm^{-1} blue-shifted from the pump beam used, epr-SRS measurements of solutions of

β-carotene in DMSO-d_6 with concentrations as low as 18 μM clearly show two vibrational resonances expected in the probed vibrational region, Fig. 4(e).

In conclusion, we have demonstrated an experimental scheme for recording spectra over the whole range of molecular vibrational resonances using epr-SRS with visible excitation. With this approach, sensitivities comparable to fluorescence imaging are realized. While moving the excitation to shorter wavelengths might lead to a higher risk of photodamage,[24] the sensitivity enhancement is high enough that excitation intensities can be reduced to an acceptable level.[25] In addition, stretching the pulses with the employed spectral focusing gives another handle on reducing potential phototoxicity. We, thus, expect that epr-SRS microscopy with visible excitation will, in the future, find numerous applications for the investigation of labeled and unlabeled biological samples.

See the supplementary material for a description of the recording of epr-SRS spectra, the spectroscopic characterization of the chromophores used, the processing of imaging data, and the preparation of samples for imaging experiments.

AUTHOR DECLARATIONS

Conflict of Interest

D.G., G.M., D.P., D.S, and L.K. are employees of the commercial laser manufacturer Light Conversion.

Author Contributions

Ashwin J. X. Choorakuttil: Data curation (equal); Formal analysis (equal); Investigation (equal); Methodology (equal); Writing – original draft (equal). **Andreas Zumbusch:** Conceptualization (lead); Funding acquisition (lead); Supervision (equal); Writing – original draft (equal); Writing – review & editing (lead). **Andrea Pruccoli:** Data curation (equal); Formal analysis (equal); Investigation (equal); Methodology (equal); Writing – original draft (equal). **Martin Josef Winterhalder:** Conceptualization (supporting); Supervision (equal). **Peyman Zirak:** Conceptualization (supporting); Investigation (supporting). **Dominykas Gudavicius:** Methodology (equal). **Giedrius Martynaitis:** Methodology (equal). **Dalius Petrulionis:** Methodology (equal). **Danielius Samsonas:** Methodology (equal). **Lukas Kontenis:** Methodology (equal); Supervision (equal).

DATA AVAILABILITY

The data that support the findings of this study are available within the article and its supplementary material.

REFERENCES

[1]M. Pilling and P. Gardner, "Fundamental developments in infrared spectroscopic imaging for biomedical applications," Chem. Soc. Rev. **45**, 1935–1957 (2016).

[2]L. Opilik, T. Schmid, and R. Zenobi, "Modern Raman imaging: Vibrational spectroscopy on the micrometer and nanometer scales," Annu. Rev. Anal. Chem. **6**, 379–398 (2013).

[3]C. Y. Chung, J. Boik, and E. O. Potma, "Biomolecular imaging with coherent nonlinear vibrational microscopy," Annu. Rev. Phys. Chem. **64**, 77–99 (2013).

[4]C. H. Camp and M. T. Cicerone, "Chemically sensitive bioimaging with coherent Raman scattering," Nat. Photonics **9**, 295–305 (2015).

[5]L. Wei, Z. Chen, L. Shi, R. Long, A. V. Anzalone, L. Zhang, F. Hu, R. Yuste, V. W. Cornish, and W. Min, "Super-multiplex vibrational imaging," Nature **544**, 465–470 (2017).

[6]L. Wei and W. Min, "Electronic preresonance stimulated Raman scattering microscopy," J. Phys. Chem. Lett. **9**, 4294–4301 (2018).

[7]A. Albrecht and M. Hutley, "On the dependence of vibrational Raman intensity on the wavelength of incident light," J. Chem. Phys. **55**, 4438–4443 (1971).

[8]P. M. Champion and A. C. Albrecht, "Resonance Raman scattering: The multi-mode problem and transform methods," Annu. Rev. Phys. Chem. **33**, 353–376 (1982).

[9]S. A. Asher, "UV resonance Raman studies of molecular structure and dynamics: Applications in physical and biophysical chemistry," Annu. Rev. Phys. Chem. **39**, 537–588 (1988).

[10]P. Fimpel, A. J. X. Choorakuttil, A. Pruccoli, L. Ebner, S. Tanaka, Y. Ozeki, M. J. Winterhalder, and A. Zumbusch, "Double modulation SRS and SREF microscopy: Signal contributions under pre-resonance conditions," Phys. Chem. Chem. Phys. **22**, 21421–21427 (2020).

[11]M. Zhuge, K.-C. Huang, H. J. Lee, Y. Jiang, Y. Tan, H. Lin, P.-T. Dong, G. Zhao, D. Matei, Q. Yang, and J.-X. Cheng, "Ultrasensitive vibrational imaging of retinoids by visible preresonance stimulated Raman scattering microscopy," Adv. Sci. **8**, 2003136 (2021).

[12]C. W. Freudiger, W. Min, B. G. Saar, S. Lu, G. R. Holtom, C. W. He, J. C. Tsai, J. X. Kang, and X. S. Xie, "Label-free biomedical imaging with high sensitivity by stimulated Raman scattering microscopy," Science **322**, 1857–1861 (2008).

[13]C. Riek, C. Kocher, P. Zirak, C. Kölbl, P. Fimpel, A. Leitenstorfer, A. Zumbusch, and D. Brida, "Stimulated Raman scattering microscopy by Nyquist modulation of a two-branch ultrafast fiber source," Opt. Lett. **41**, 3731–3734 (2016).

[14]Y. L. Bi, C. Yang, Y. G. Chen, S. Yan, G. Yang, Y. Z. Wu, G. P. Zhang, and P. Wang, "Near-resonance enhanced label-free stimulated Raman scattering microscopy with spatial resolution near 130 nm," Light: Sci. Appl. **7**, 81 (2018).

[15]T. Hellerer, A. M. Enejder, and A. Zumbusch, "Spectral focusing: High spectral resolution spectroscopy with broad-bandwidth laser pulses," Appl. Phys. Lett. **85**, 25–27 (2004).

[16]W. Langbein, I. Rocha-Mendoza, and P. Borri, "Coherent anti-Stokes Raman micro-spectroscopy using spectral focusing: Theory and experiment," J. Raman Spectrosc. **40**, 800–808 (2009).

[17]H. Watanabe, N. Hayazawa, Y. Inouye, and S. Kawata, "DFT vibrational calculations of rhodamine 6G adsorbed on silver: Analysis of tip-enhanced Raman spectroscopy," J. Phys. Chem. B **109**, 5012–5020 (2005).

[18]R. Jakobsen, "The vibrational spectra of benzonitrile–d_5," Spectrochim. Acta **21**, 127–131 (1965).

[19]P. Berto, E. R. Andresen, and H. Rigneault, "Background-free stimulated Raman spectroscopy and microscopy," Phys. Rev. Lett. **112**, 053905 (2014).

[20]M. Andreana, M.-A. Houle, D. J. Moffatt, A. Ridsdale, E. Buettner, F. Legare, and A. Stolow, "Amplitude and polarization modulated hyperspectral stimulated Raman scattering microscopy," Opt. Express **23**, 28119–28131 (2015).

[21]T. Behnke, C. Würth, E.-M. Laux, K. Hoffmann, and U. Resch-Genger, "Simple strategies towards bright polymer particles via one-step staining procedures," Dyes Pigm. **94**, 247–257 (2012).

[22]A. B. Neef and N. W. Luedtke, "An azide-modified nucleoside for metabolic labeling of DNA," ChemBioChem **15**, 789–793 (2014).

[23]A. Pruccoli, M. Kocademir, M. J. Winterhalder, and A. Zumbusch, "Electronically preresonant stimulated Raman scattering microscopy of weakly fluorescing chromophores," J. Phys. Chem. B **127**, 6029–6037 (2023).

[24]B. Talone, M. Bazzarelli, A. Schirato, F. D. Vicario, D. Viola, E. Jacchetti, M. Bregonzio, M. T. Raimondi, G. Cerullo, and D. Polli, "Phototoxicity induced in living HeLa cells by focused femtosecond laser pulses: A data-driven approach," Biomed. Opt. Express **12**, 7886–7905 (2021).

[25]C. W. Freudiger, W. L. Yang, G. R. Holtom, N. Peyghambarian, X. S. Xie, and K. Q. Kieu, "Stimulated Raman scattering microscopy with a robust fibre laser source," Nat. Photonics **8**, 153–159 (2014).